

Simulating neuronal dynamics in fractional adaptive exponential integrate-and-fire models

Alexandru Fikl^{a,*}, Aman Jhinga^b, Eva Kaslik^b, Argha Mondal^c

^a Institute for Advanced Environmental Research, West University of Timișoara, 300086, Romania

^b Department of Mathematics and Computer Science, West University of Timișoara, Timișoara 300223, Romania

^c Department of Mathematics, Sidho-Kanho-Birsha University, Purulia-723104, WB, India

Abstract

We introduce an efficient discretization of a novel fractional-order adaptive exponential (FrAdEx) integrate-and-fire model, which is used to study the fractional-order dynamics of neuronal activities. The discretization is based on extension of L1-type methods that can accurately handle the exponential growth and the spiking mechanism of the model. This new method is implicit and uses adaptive time stepping to robustly handle the stiff system that arises due to the exponential term. The implicit nonlinear system can be solved exactly, without the need for iterative methods, making the scheme efficient while maintaining accuracy. We present a complete error model for the numerical scheme that can be extended to other integrate-and-fire models with minor changes. To show the feasibility of our approach, the numerical method has been rigorously validated and used to investigate several different spiking oscillations of the model. We observed that the fractional-order model is capable of predicting biophysical activities, which are interpreted through phase diagrams describing the transition from one firing type to another. This simple model shows significant promise, as it has sufficient expressive dynamics to reproduce several features qualitatively from a biophysical dynamical perspective.

Keywords: fractional derivatives; integrate-and-fire model; L1 method; adaptive time stepping.

1. Introduction

The adaptive exponential (AdEx) integrate-and-fire model [1] holds an important position in the field of computational neuroscience, serving as a bridge between simplified neuron models and highly complex real-world neuronal dynamics [2, 3]. Originating from classical integrate-and-fire models [4, 5], the AdEx variant incorporates several mechanisms to better replicate the spiking patterns of real biological neurons [6]. To further enhance the fidelity of the AdEx models, authors have recently looked at introducing non-standard operators with desirable properties, such as fractional derivatives [7].

*Corresponding Author

Email address: alexandru.fikl@e-uvv.ro (Alexandru Fikl)

Its precursor, the traditional leaky integrate-and-fire model [4], has been widely employed as a simple representation of spiking neurons, but has showcased multiple limitations. To address these limitations, researchers have proposed generalisations in three distinct directions. Firstly, the model was extended to incorporate non-linear components, such as quadratic [8] or exponential terms [9]. This modification allows replacing the strict voltage threshold with a more realistic smooth spike initiation zone, which better resembles the behaviour of real neurons. Secondly, an additional variable has been introduced into the model [10], which accounts for sub-threshold resonances or adaptation mechanisms. Sub-threshold resonances capture how a neuron's response to input varies with input frequency and adaptation mechanisms reflect changes in a neuron's firing rate or behaviour in response to prolonged stimulation. A third direction involves changing the stimulation paradigm from current injection to conductance injection with the aim of bringing integrate-and-fire models closer to the conditions experienced by cortical neurons in vivo [11, 9]. Conductance injection takes into consideration the dynamic changes in synaptic conductance that occur in real neuronal networks, enhancing the physiological relevance of the model. These extensions have been incorporated into the AdEx model, making it more suitable for simulating the behaviour of spiking neurons in diverse biological systems.

Detailed conductance-based models, such as Hodgkin-Huxley-type models, have also been employed to investigate electrophysiological phenomena [12, 13]. However, these models pose challenges for direct mathematical analysis, numerical implementation, and the replication of experimental spike patterns. Therefore, studies of integrate-and-fire models, such as the AdEx model, have been performed and have shown promising results compared to more complex neuron models [1, 14]. In particular, they demonstrate their effectiveness in reproducing the behaviour of layer-V neocortical pyramidal neurons under random stimuli [15].

Very recently, an extension of the AdEx model has been proposed in [16], which involves replacing the standard integer-order derivative with a so-called (local) fractal derivative. The study suggests that the fractal derivative orders significantly influence inter-spike intervals and mean firing frequencies, potentially offering a more accurate representation of neuronal activity. We investigate here a similar extension involving the fractional (Caputo) derivative, which lends itself to a more rigorous mathematical analysis. The relevance of time-fractional calculus has grown immensely in various interdisciplinary fields over the past few decades due to its ability to incorporate memory effects and hereditary characteristics inherent in many physical systems [17, 18]. Fractional systems have also been found to exhibit richer dynamics than some of their integer-order counterparts [19, 20]. As such, fractional calculus has been effectively employed in modelling a wide spectrum of phenomena, from anomalous transport in porous media [21, 22] to complex behaviours observed in biological systems [23, 24, 25].

Incorporating fractional derivatives into integrate-and-fire neuronal models introduces a new mathematical tool directed at capturing the nonlocal, history-dependent behaviour of neuronal dynamics. Traditional models, based on integer-order derivatives, fall short in modelling memory effects and continuous integration of past neuronal states. This limitation is linked to the inability of classical models to simulate long-term dependencies or anomalous propagation behaviour [21, 22] that are characteristics of certain neuronal systems. To address these challenges, a fractional

order leaky integrate-and-fire model was introduced [7], recognising that neuronal voltage trajectories often exhibit dynamics across multiple time scales [26, 27]. These dynamics, indicative of complex intracellular interactions, often follow power-law behaviours that may be efficiently modelled by fractional differential equations [28].

In this paper, we describe a fractional-order adaptive exponential (FrAdEx) model, designed to investigate the fractional-order dynamics that govern neuronal activity. As shown, the FrAdEx model (1) with the reset condition (2) is an impulsive system of (Caputo-type) fractional differential equations with state-dependent impulses. Impulsive differential equations offer a valuable mathematical framework for investigating evolutionary processes characterised by abrupt and sudden state changes. They can be categorised into two main classes based on their impulsive events: fixed-time impulsive systems and state-dependent impulsive systems. Although extensive research efforts have been dedicated to the study of fixed-time impulsive systems [29], it is crucial to acknowledge that in the real world many systems do not experience impulses at predetermined fixed intervals, but rather in response to specific states [30, 31]. To the best of our knowledge, there are currently no published results in the literature regarding the theoretical and numerical analysis of fractional-order impulsive systems with state-dependent impulses.

Consequently, the objective of this paper is to propose and investigate numerical methods tailored for the FrAdEx model. Specifically, we describe an implicit adaptive L1-type scheme engineered to address the three main challenges in simulating the FrAdEx model. Firstly, the (Caputo) fractional derivative is defined as an integral operator with a weakly singular kernel which we discretise using the standard linear interpolation of the L1 method [32]. This allows a straightforward handling of the singularity and results in an implicit numerical scheme. An implicit method is desired for the FrAdEx model due to the exponential growth in the spike initiation zone, which results in a generally stiff system. Secondly, using an implicit method is not sufficient to accurately represent the exponential growth, so the L1 method is augmented with an adaptive time-stepping scheme based on [33]. The non-uniform time step allows a fine control over the error in the exponential region and results in accurate estimates of the spike times. The third issue is common to state-dependent impulsive systems and requires an accurate representation of the reset condition as the neuron produces spikes. Discretizations of integer-order integrate-and-fire models have been investigated in [34], where a high-order approximation of the spike times and reset is provided. However, such extensions are not possible for the FrAdEx model due to the memory properties of the fractional derivative. Therefore, we present an estimate of the spike times based on the Lambert W function that does not require iteration. High-order methods for fractional differential equations have also been developed [32, 35, 36], but much less attention has been shown to the fully non-uniform case required here. As such, significant effort will be required to extend the current discretization to higher-order. The first-order method presented here features enhanced stability properties and a complete error model that can be extended to other integrate-and-fire-type models with minor modifications.

The structure of the paper is as follows. In Section 2, we will introduce the FrAdEx model and describe its parameters and general construction. In Section 3, we will briefly define the necessary fractional calculus concepts and notation to interpret the FrAdEx model, which is used in Section 4 to present a nondimensional version of the model that is used in simulations. Then, Section 5 describes the L1-type scheme used to discretise the model and

the specific handling of the state-dependent impulses. The stability and convergence of the method is analysed in Section 6. We then verify and validate the method on multiple integrate-and-fire models and show its performance properties in Section 7. In Section 8, we show that the newly introduced FrAdEx model can numerically reproduce known phenomenological responses of neurons for several parameter ranges. Finally, we discuss the conclusions in Section 9.

2. Model

The fractional-order model we consider here is a straightforward extension of the standard integer-order AdEx model from [2]. This extension is common in capacitance-based models and relies on the generalisation of Curie's empirical law described in [37]. It is given by

$$\begin{aligned} C \frac{d^{\alpha_1} V}{dt^{\alpha_1}} &= I - g_L(V - E_L) + g_L \Delta_T \exp\left(\frac{V - V_T}{\Delta_T}\right) - w, \\ \tau_w \frac{d^{\alpha_2} w}{dt^{\alpha_2}} &= a(V - E_L) - w, \end{aligned} \quad (1)$$

under suitable initial conditions with fractional orders $0 < \alpha_i < 1$, not necessarily equal (for details, see Section 3). The FrAdEx model describes the evolution of the membrane voltage potential $V(t)$, driven by an external current $I(t)$, and an adaptation variable $w(t)$. The model is constructed such that when the voltage potential increases beyond the parameter value V_T , the exponential term in the first equation activates a positive feedback for spike generation. In integrate-and-fire models, this exponential increase in the potential is truncated at a threshold value V_{peak} , which is used to denote the generation of an action potential. At this point, the voltage is reset to a fixed value V_r and the adaptation variable w is updated by a fixed offset b . In physical systems, the neuron exhibits a spike if V grows rapidly. However, in the FrAdEx model, a spike is generated only when it reaches the threshold value V_{peak} . This may shift spike times by a very small time duration (milliseconds) compared to experiments [15, 2]. The model (1) uses the following reset condition to control the upswing and downswing of the membrane potential

$$\text{if } V > V_{\text{peak}} \text{ then } \begin{cases} V \leftarrow V_r, \\ w \leftarrow w + b. \end{cases} \quad (2)$$

The parameters describing the model are divided into so-called *scaling* parameters and *bifurcation* parameters. The scaling parameters are responsible for scaling the time axis and scaling (or offsetting) the system variables [2]. The five scaling parameters are the total capacitance C , the total leak conductance g_L , the effective resting potential E_L , the threshold slope factor Δ_T , and the effective threshold potential V_T . The bifurcation parameters are directly proportional to the time constant τ_w , the conductance a , the spike triggered adaptation b and the reset potential V_r . These parameters are responsible for changes in the qualitative neuronal activities (such as multiple firings). For example, the parameter a controls the sensitivity of the adaptation current to the membrane voltage.

3. Fractional Calculus Background

We give here a short introduction to the notation used throughout the remaining sections and motivate the choice of fractional derivative operators. For simplicity, we denote the fractional model (1) of order $\alpha \in (0, 1)^2$ in vector form as

$$\frac{d^\alpha \mathbf{y}}{dt^\alpha} = \mathbf{f}(t, \mathbf{y}),$$

where $\mathbf{y} \triangleq (V, w)$ and $\mathbf{f} : \mathbb{R}_+ \times \mathbb{R}^2 \rightarrow \mathbb{R}^2$ is the right-hand side. We also denote by τ_m , for $m \in \{0, \dots, M\}$, the $M + 1$ spike times that occur in the system, with the convention that $\tau_0 = 0$ and $\tau_N = T$ denote the domain limits. The interior spikes $\tau_m(\mathbf{y})$, for $m \in \{1, \dots, M - 1\}$, are state-dependent and are not known a priori. We also use the notation $AC([0, T]; \mathbb{R}^n)$ to denote the space of absolutely continuous functions and $PAC([0, T]; \mathbb{R}^n)$ to denote the space of piecewise absolutely continuous functions on $[0, T]$ with values in \mathbb{R}^n . The standard notation $PAC^k([0, T], \mathbb{R}^n)$ is used to denote functions that are piecewise differentiable k times and each derivative is absolutely continuous. For impulsive systems, the solutions are found in the $PAC^k([0, T]; \mathbb{R}^n)$ space due to the reset condition. To handle the vector system, we make use of standard multi-index notation, where operations are applied component-wise, unless indicated.

The choice of fractional derivative in (1) is also a choice that must be made in the modelling process. In this work, we focus on the Caputo derivative, which is classically defined for $\mathbf{y} \in AC([0, T]; \mathbb{R}^2)$ by [38]

$${}^C D_{0^+}^\alpha [\mathbf{y}](t) \triangleq \frac{1}{\Gamma(1 - \alpha)} \int_0^t \frac{\mathbf{y}'(s)}{(t - s)^\alpha} ds,$$

for $t > 0$. The Caputo derivative is often used in physical systems because it has several attractive qualities, such as local initial conditions and the fact that the derivative of a constant vanishes [38]. This definition can be extended to the case of $\mathbf{y} \in PAC([0, T]; \mathbb{R}^2)$, as shown in [39]. We have that

$${}^{PC} D_{0^+}^\alpha [\mathbf{y}](t) \triangleq \frac{1}{\Gamma(1 - \alpha)} \left[\sum_{j=0}^{m-1} \int_{\tau_j}^{\tau_{j+1}} \frac{\mathbf{y}'(s)}{(t - s)^\alpha} ds + \int_{\tau_m}^t \frac{\mathbf{y}'(s)}{(t - s)^\alpha} ds \right], \quad (3)$$

for $t \in (\tau_m, \tau_{m+1}]$. According to [39, Lemma 2.7], we can write the impulsive system in Volterra integral equation form as

$$\mathbf{y}(t) = \mathbf{y}_0 + \sum_{j=1}^m [\mathbf{y}(\tau_j^+) - \mathbf{y}(\tau_j^-)] + \frac{1}{\Gamma(\alpha)} \int_0^t \frac{\mathbf{f}(s, \mathbf{y}(s))}{(t - s)^{1-\alpha}} ds, \quad (4)$$

where the one-sided limits are defined as

$$y(\tau_m^\pm) \triangleq \lim_{\epsilon \rightarrow 0^+} y(\tau_m \pm \epsilon).$$

In practice, both formulations can be used in the construction of a numerical method. However, for the FrAdEx model, we prefer discretising the Caputo derivative directly, as it avoids the summation over the exponential right-hand side and gives rise to implicit methods, which allow for larger time steps.

Remark 3.1. For the FrAdEx model (2), we have a constant jump at each spike time, i.e., $\mathbf{y}(\tau_m^+) - \mathbf{y}(\tau_m^-) = \Delta \mathbf{y} \triangleq (V_r - V_{\text{peak}}, b)$. Therefore, we can write

$$\mathbf{y}(t) = \mathbf{y}_0 + m\Delta \mathbf{y} + \frac{1}{\Gamma(\alpha)} \int_0^t \frac{\mathbf{f}(s, \mathbf{y}(s))}{(t-s)^{1-\alpha}} ds.$$

Remark 3.2. The Riemann–Liouville derivative can also be used in the definition of (1). In the piecewise-continuous case, we have that [40, Definition 2.4]

$${}^{PRL}D_{0+}^\alpha[\mathbf{y}](t) = {}^{PC}D_{0+}^\alpha[\mathbf{y}](t) + \frac{1}{\Gamma(1-\alpha)} \frac{\mathbf{y}(\tau_0^+)}{t^\alpha} + \frac{1}{\Gamma(1-\alpha)} \sum_{j=1}^m \frac{\mathbf{y}(\tau_j^+) - \mathbf{y}(\tau_j^-)}{(t-\tau_j)^\alpha},$$

for $t \in (\tau_m, \tau_{m+1}]$. However, while the Riemann–Liouville derivative requires less regularity in the solutions, it also requires nonlocal initial conditions [38].

4. Non-Dimensional Model

The model (1) can be non-dimensionalized to reduce the parameter space to only 4 parameters in the equations and the 3 parameters in the reset condition. We provide here a non-dimensionalization that we use going forward to simplify the description and analysis of the numerical methods. We follow the suggestion from [2] and define the non-dimensional variables

$$\bar{t} \triangleq \frac{\alpha_1 \sqrt{gL}}{C} t, \quad \bar{V} \triangleq \frac{V - V_T}{\Delta_T} \quad \text{and} \quad \bar{w} \triangleq \frac{w}{\Delta_T gL}.$$

This choice of non-dimensionalization is specific to the fractional case, where the Caputo derivative itself has units of $s^{-\alpha}$. Replacing these relations into our original model (1), we obtain

$$\begin{cases} \frac{d^{\alpha_1} \bar{V}}{d\bar{t}^{\alpha_1}} = \bar{I} - (\bar{V} - \bar{E}_L) + \exp(\bar{V}) - \bar{w}, \\ \bar{\tau}_w \frac{d^{\alpha_2} \bar{w}}{d\bar{t}^{\alpha_2}} = \bar{a}(\bar{V} - \bar{E}_L) - \bar{w}, \end{cases} \quad (5)$$

where

$$\bar{I} \triangleq \frac{I}{\Delta_T gL}, \quad \bar{E}_L \triangleq \frac{E_L - V_T}{\Delta_T}, \quad \bar{\tau}_w \triangleq \left(\frac{gL}{C}\right)^{\frac{\alpha_2}{\alpha_1}} \tau_w \quad \text{and} \quad \bar{a} \triangleq \frac{a}{gL}.$$

We also obtain the non-dimensional reset condition

$$\bar{V} > \bar{V}_{\text{peak}} \quad \text{then} \quad \begin{cases} \bar{V} \leftarrow \bar{V}_r, \\ \bar{w} \leftarrow \bar{w} + \bar{b}, \end{cases} \quad (6)$$

where

$$\bar{V}_{\text{peak}} \triangleq \frac{V_{\text{peak}} - V_T}{\Delta_T}, \quad \bar{V}_r \triangleq \frac{V_r - V_T}{\Delta_T}, \quad \text{and} \quad \bar{b} \triangleq \frac{b}{\Delta_T gL}.$$

Remark 4.1. Equation (5) and the reset condition (6) will be used from this point onwards. To simplify the notation, we will drop the overline notation (e.g. \bar{V}) in the following with the understanding that the variables are all non-dimensional.

5. Numerical Methods

For the discretization of the FrAdEx model (5), we use an L1-type method on a non-uniform grid, to accurately account for the exponential growth of the solutions and the discontinuous spiking. For a complete description and analysis of the standard L1 method see classic monographs such as [32]. Following the same ideas, we use a linear approximation of the function in each interval, i.e. for $s \in [t_n, t_{n+1}]$ we have that

$$\mathbf{y}(s) \approx \frac{t_{n+1} - s}{t_{n+1} - t_n} \mathbf{y}_n^+ + \frac{s - t_n}{t_{n+1} - t_n} \mathbf{y}_{n+1}^- \implies \mathbf{y}'(s) \approx \frac{\mathbf{y}_{n+1}^- - \mathbf{y}_n^+}{t_{n+1} - t_n},$$

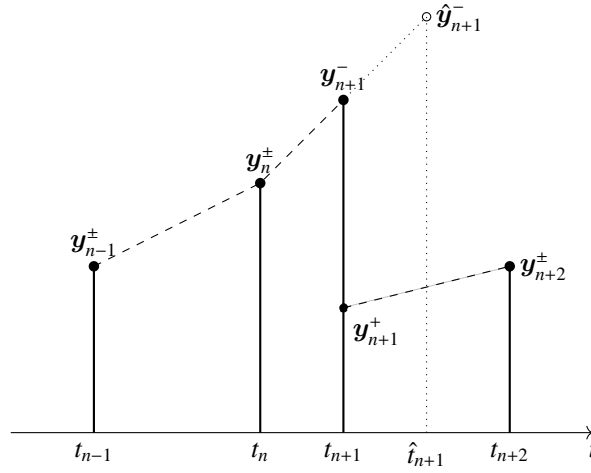


Figure 1: Reconstruction of the solution at a spike. The initial guess $\hat{\mathbf{y}}_{n+1}^-$ is pulled back to the approximated time t_{n+1} , where the discontinuous spike occurs.

where \mathbf{y}_n^\pm denote the the right and left-sided limits, respectively, at t_n . The two values are different when a numerical spike has been inserted at time t_n (see Figure 1). This results in the following discrete form of the system (5)

$$\sum_{k=0}^n \mathbf{d}_{n+1,k} \odot \frac{\mathbf{y}_{k+1}^- - \mathbf{y}_k^+}{\Delta t_k} = \mathbf{f}(t_{n+1}, \mathbf{y}_{n+1}^-), \quad (7)$$

where \odot denotes the component-wise Hadamard product. The weights are given by

$$(\mathbf{d}_{n+1,k})_i \triangleq \frac{(t_{n+1} - t_k)^{1-\alpha_i} - (t_{n+1} - t_{k+1})^{1-\alpha_i}}{\Gamma(2 - \alpha_i)}. \quad (8)$$

By construction, the method is implicit and the solution \mathbf{y}_{n+1}^- must be obtained by finding the root of the nonlinear equation

$$\mathbf{y}_{n+1}^- - \mathbf{h}_{n+1} \odot \mathbf{f}(t_{n+1}, \mathbf{y}_{n+1}^-) = \mathbf{y}_n^+ - \mathbf{h}_{n+1} \odot \sum_{k=0}^{n-1} \mathbf{d}_{n+1,k} \odot \frac{\mathbf{y}_{k+1}^- - \mathbf{y}_k^+}{\Delta t_k},$$

where $(\mathbf{h}_{n+1})_i = \Delta t_n / (\mathbf{d}_{n+1,n})_i = \Gamma(2 - \alpha_i) \Delta t_n^{\alpha_i}$.

However, as is, the discretization does not yet take into account the reset condition (6). In practical terms, in (7) we can encounter a reset in the current time interval $[t_n, t_{n+1}]$. To maintain the requirement that the numerical spike

times occur at interval boundaries, we recompute t_{n+1} to ensure that the solution remains piecewise continuous, as shown in Figure 1. Therefore, both y_{n+1}^- and t_{n+1} are provisional in this equation and may be modified by the end of the time step. To emphasise this fact, we rewrite the equation as

$$\hat{y}_{n+1}^- - \hat{h}_{n+1} \odot \mathbf{f}(\hat{t}_{n+1}, \hat{y}_{n+1}^-) = \mathbf{y}_n^+ - \hat{h}_{n+1} \odot \sum_{k=0}^{n-1} \hat{d}_{n+1,k} \odot \frac{\mathbf{y}_{k+1}^- - \mathbf{y}_k^+}{\Delta t_k} = \hat{r}_{n+1}, \quad (9)$$

where the hat terms denote a dependence on the yet-to-be-determined \hat{t}_{n+1} . The complete pseudocode of the algorithm that evolves the solution to the next time step is given in Algorithm 1.

Algorithm 1 L1 method for FrAdEx integrate-and-fire models.

Require: Derivative order α and time span $[0, T]$.

Require: I.C. \mathbf{y}_0 , parameters (I, E_L, τ_w, a) from (5), and $(V_{\text{peak}}, V_r, b)$ from (6).

Require: Initial step Δt_0 and adaptive algorithm parameters from Section 5.3.

while $t_n \leq T$ **do**

1. Solve (9) using methods from Section 5.1.

2. If \hat{V}_{n+1}^- is real, continue to step 4 with $t_{n+1} \equiv \hat{t}_{n+1}$ and

$$(\mathbf{y}_{n+1}^-, \mathbf{y}_{n+1}^+) = (\hat{y}_{n+1}^-, \hat{y}_{n+1}^-).$$

3.1 If \hat{V}_{n+1}^- is complex, compute a step according to Section 5.2 and set

$$t_{n+1} = t_n + \Delta t_{\text{Lambert}}.$$

3.2 If $t_{n+1} - t_n \leq \Delta t_{\text{min}}$, assume a spike occurred and set

$$(V_{n+1}^-, V_{n+1}^+) = (V_{\text{peak}}, V_r),$$

$$(w_{n+1}^-, w_{n+1}^+) = (c_0 V_{\text{peak}} + c_1, c_0 V_{\text{peak}} + c_1 + b),$$

where c_0 and c_1 are defined in (10). Continue to step 5 (step accepted).

4. $h \leftarrow \text{DetermineTimestep}(t_0, \mathbf{y}_0^\pm), \dots, (t_{n+1}, \mathbf{y}_{n+1}^\pm)$ using Section 5.3.

5. If the step is accepted, continue to the the next step with $\Delta t_{n+1} = h$;
otherwise retry the step with $\Delta t_n = h$ *without* updating the solution.

end while

In Section 5.1, we describe a solution method for (9) that does not require an iterative solver, but instead relies on computing the special Lambert W function. The Lambert W function can also be used to bound the allowable time step Δt_{n+1} , which is described in Section 5.2. Finally, an adaptive time-stepping algorithm is described in Section 5.3.

5.1. Lambert W Solution

The evolution equation (9) is implicit and must be solved for the value of \mathbf{y}_{n+1}^- (and \mathbf{y}_{n+1}^+ according to Algorithm 1). While this can be done by iterative Newton–Raphson-type methods, it is not necessarily for this class of adaptive exponential integrate-and-fire models, as an analytical solution can be obtained. The equation can be written component-wise, while expanding the right-hand side from (5),

$$\begin{aligned}\hat{V}^- &= \hat{h}_V \left(I - (\hat{V}^- - E_L) + \exp(\hat{V}^-) - \hat{w}^- \right) + \hat{r}_V, \\ \hat{w}^- &= \frac{\hat{h}_w}{\tau_w} \left(a(\hat{V}^- - E_L) - \hat{w}^- \right) + \hat{r}_w,\end{aligned}$$

where we have dropped the $n + 1$ index to simplify the notation. We can see here that the second equation can be solved for \hat{w}^- for a known \hat{V}^- . We have that

$$\hat{w}^- = \frac{a\hat{h}_w}{\hat{h}_w + \tau_w} \hat{V}^- + \frac{\tau_w \hat{r}_w - a\hat{h}_w E_L}{\hat{h}_w + \tau_w} \triangleq c_0 \hat{V}^- + c_1,$$

which we can then replace into the \hat{V}^- equation to obtain

$$\hat{V}^- + c_2 = c_3 \exp(\hat{V}^-),$$

where

$$c_2 = \frac{\hat{h}_V(I + E_L - c_1) + \hat{r}_V}{1 + \hat{h}_V(1 + c_0)} \quad \text{and} \quad c_3 = \frac{\hat{h}_V}{1 + \hat{h}_V(1 + c_0)}.$$

This equation has a known analytical solution in terms of the Lambert W function. Therefore, the final solution is written as

$$\begin{cases} \hat{V}^- = -c_2 - W[-c_3 \exp(-c_2)], \\ \hat{w}^- = c_0 \hat{V}^- + c_1. \end{cases} \quad (10)$$

5.2. Time Step Limit

The Lambert W-based solution (10) also provides an accurate method to approximate the maximum allowable time step when approaching a spike. By definition, we know that the Lambert W function gives a complex-valued solution to $y = xe^x$. If we require the solution to be real, then

$$x = \begin{cases} W_0(y), & 0 \leq y, \\ W_0(y), W_{-1}(y), & -\frac{1}{e} \leq y < 0, \end{cases}$$

where $W_k(y)$ denotes the k -th branch of the Lambert W function. We can see that on $-1/e \leq y < 0$ the solution is multivalued, with the property that

$$W_0(y) \geq W_{-1}(y), \quad \forall y \in \left(-\frac{1}{e}, 0\right),$$

so the $k = 0$ branch is always larger on the given interval. When considering the two branches in (10), we always choose the $k = 0$ branch, as it results in a smaller change in \hat{V}^- and is consistent in the limit of $\Delta t_n \rightarrow 0$.

Therefore, ensuring that the argument of the Lambert W function is at most equal to the lower bound $-1/e$ will result in an equivalent bound on the allowable time step $\Delta t_n \leq \Delta t_{\text{Lambert}}$. Following (10), we require that

$$-\frac{1}{e} \leq -c_3 \exp(-c_2) < 0.$$

Remark 5.1. *We have that*

$$c_3 = \frac{\hat{h}_V}{1 + \hat{h}_V(1 + c_0)} > 0 \iff a \geq -\frac{\hat{h}_w + \tau_w}{\hat{h}_w} \frac{1 + \hat{h}_V}{\hat{h}_V},$$

where $\hat{h}_V, \hat{h}_w, \tau_w > 0$. In the limit of small Δt_n , the inequality is satisfied for all parameters (a, τ_w) of physical significance (see [2, Table 1]), so we assume $c_3 > 0$.

Assuming that $c_3 > 0$, the condition can be simplified to

$$0 < c_3 \exp(-c_2 + 1) \leq 1, \tag{11}$$

where the left inequality is satisfied automatically and the right inequality can be used to estimate a maximum allowable time step. Then, to obtain this time step we must find the root of the following nonlinear equation

$$c_3(\Delta t^*) \exp(-c_2(\Delta t^*) + 1) = 1,$$

for $\Delta t^* \in [0, \hat{t}_{n+1} - t_n]$. However, this can be very inefficient due to the fact that the time step Δt^* appears in the memory terms \hat{r}_{n+1} (9), which would need to be recomputed at each iteration of the optimisation problem. In practice, we consider that the memory terms do not depend explicitly on the time step. This gives an upper bound on the time step that is not optimal in the sense of (11), but gives sufficiently good results. Then, the Lambert W-based maximum time step estimate is set to

$$\Delta t_{\text{Lambert}} = \Delta t^*.$$

Remark 5.2. *The optimisation problem required to find Δt^* can be solved efficiently. The argument of the Lambert W function is well behaved as a function of Δt^* and we know that the solution is tightly bracketed in $[0, \hat{t}_{n+1} - t_n]$.*

Remark 5.3. *If the assumption that the memory terms do not depend on the time step is seen as prohibitive, the algorithm can always fall back to solely making use of the adaptive algorithm described in Section 5.3. This may result in a poorer approximation of the spike times, but the method itself maintains the error estimates provided in Section 6.*

5.3. Adaptive Time Step

Due to the exponential growth near the generation of an action potential, as seen in the results from [2], an accurate solution to (5) requires an adaptive time-stepping method. Adaptive methods are well developed for the integer order case [41], where the truncation error can be used to give accurate approximations of the required time steps. However, equivalent methods have not yet been developed for fractional-order evolution equations. A notable exception is the

recent work from [33], which introduces a simple error indicator with good properties for fractional equations. Here, we give a short description of the adaptive algorithm.

The error estimator derived in [33] is given by

$$\chi_{n+1} \triangleq \Gamma(1 + \alpha) \frac{t_{n+1} - t_n}{t_{n+1}^\alpha - t_n^\alpha} \frac{\|\mathbf{y}_{n+1} - \mathbf{y}_n\|}{\|\mathbf{y}_n\|},$$

for a chosen norm $\|\cdot\|$. The error χ_{n+1} is expected to be maintained between $\chi_{\min} < \chi_{n+1} < \chi_{\max}$. As written, this error estimator has a few downsides: it has units of $s^{1-\alpha}$ and does not apply directly to the case of different orders α for each component. Therefore, we propose a simple extension in the form of

$$\hat{\chi}_{n+1} \triangleq \|\Gamma(1 + \alpha)\| \frac{(t_{n+1} - t_n)^\alpha}{t_{n+1}^\alpha - t_n^\alpha} \frac{\|\mathbf{y}_{n+1} - \mathbf{y}_n\|}{\|\mathbf{y}_n\|} \implies \chi_{n+1} \triangleq \frac{\hat{\chi}_{n+1} - \chi_{\min}}{\chi_{\max} - \chi_{\min}}. \quad (12)$$

The new χ_{n+1} estimator has normalised values in $[0, 1]$, based on the reference values χ_{\min} and χ_{\max} , and is non-dimensional. Then, the adaptive algorithm follows the steps from [33]:

1. Compute the estimator χ_{n+1} from (12).
2. If $0 < \chi_{n+1} < 1$, set $\Delta t_{n+1} = \theta \Delta t_n$, for a safety factor $\theta \in (0, 1]$ close to 1.
3. If $\chi_{n+1} < 0$, the step is accepted and can be increased by setting $\Delta t_{n+1} = \rho \Delta t_n$, for $\rho > 1$.
4. If $\chi_{n+1} > 1$, the step is rejected and must be decreased by setting $\Delta t_{n+1} = \sigma \Delta t_n$, for $\sigma \in (0, 1]$, subject to the requirement in step 5.
5. If $\Delta t_{n+1} < \Delta t_{\min}$, the step is accepted and we set $\Delta t_{n+1} = \Delta t_{\min}$.

As such, the algorithm has a total of 6 parameters that must be chosen based on the problem at hand. The χ_{\min} and χ_{\max} bounds are the most important, as they determine the thresholds where the time step can be increased or decreased. The analysis from [33] does not provide a robust way to choose these parameters and we do not explore this improvement.

6. Stability and Convergence

In this section, we present an error analysis of the piecewise L1 method described in Section 5, which can be applied to the FrAdEx model and other similar impulsive models. For simplicity, we only consider the scalar case, as the extension to the vector case is straightforward. The scalar equation is

$$\frac{d^\alpha y}{dt^\alpha} = f(t, y) \quad \text{if } y > y_{\text{peak}} \quad \text{then } y \leftarrow y_r, \quad (13)$$

where the right-hand side is assumed to be nonlinear and $0 < \alpha < 1$. The discretization from Section 5 applies directly to this equation and can be written as

$$y_{n+1}^- - h_{n+1} f(t_{n+1}, y_{n+1}) = y_n^+ - h_{n+1} \sum_{k=0}^{n-1} d_{n+1,k} \frac{y_{k+1}^- - y_k^+}{\Delta t_k}. \quad (14)$$

We recall that the standard L1 method has an order of $O(h^{2-\alpha})$ on a uniform mesh of spacing h for sufficiently smooth functions. On a non-uniform mesh, the analysis is provided by [42, Theorem 4.2] with $y \in C^2([0, 2])$. An extension of the results from [42] to the case of impulsive systems is trivial when the spike times $\{\tau_m\}$ are known a priori and the grid $\{t_n\}$ incorporates the discontinuities. We first define

$$\Delta t_{\max} \triangleq \max_{0 \leq n < N} \Delta t_n \quad \text{and} \quad \Delta t_{\min} \triangleq \min_{0 \leq n < N} \Delta t_n,$$

and assume that $C_{\Delta t} = \Delta t_{\max}/\Delta t_{\min}$ is finite, but can be quite large in practice (e.g. due to the exponential adaptation of (1)). We also denote by $y(t_n^\pm)$ and y_n^\pm the known continuous solution and the numerical solution, respectively.

Lemma 6.1. *Let $0 < \alpha < 1$ and $y \in \text{PAC}^2([0, T])$, with a countable set of discontinuities $\tau_1 < \dots < \tau_m < \dots < \tau_M$. Let the numerical grid $0 = t_0 < \dots < t_n < \dots < t_N = T$ be such that for every m there exists an n such that $\tau_m = t_n$. Then, for every n , it holds that*

$$\frac{d^\alpha y}{dt^\alpha}(t_{n+1}) = \sum_{k=0}^n d_{n+1,k} \frac{y(t_{k+1}^-) - y(t_k^+)}{\Delta t_k} + R_{n+1}, \quad (15)$$

and

$$|R_{n+1}| \leq \frac{1}{\Gamma(1-\alpha)} \left[\frac{\Delta t_n^{2-\alpha}}{2(1-\alpha)} + \frac{\Delta t_{\max}^2 \Delta t_n^{-\alpha}}{8} \right] \text{ess sup}_{0 \leq s \leq t_{n+1}} |y''(s)|. \quad (16)$$

Proof. See proof of [42, Theorem 4.2].

□

□

We now consider the case of interest, where the spike times $\{\tau_m\}$ are solution-dependent. Then, a grid $\{t_k\}$ that conforms to the piecewise nature of the solution cannot be constructed a priori. However, a similar error estimate can be constructed for this class of impulsive systems. We will assume that the numerical spike times are a first-order approximation of the real spike times $\{\tau_m\}$, to match the construction from Section 5. The construction of higher-order methods for models with exponential growth is left for future study.

We start by giving an estimate for truncation error below.

Theorem 6.1 (Piecewise L1 Truncation Error). *Let $0 < \alpha < 1$ and $y \in \text{PAC}^2([0, T])$, with a countable set of discontinuities $\tau_1 < \dots < \tau_m < \dots < \tau_M$. Let the numerical grid $0 = t_0 < \dots < t_n < \dots < t_N = T$ be such that for every m there exists an n such that $\tau_m \in [t_{n-1}, t_{n+1}]$. Then, for $t_{n+1} \in [\tau_m, \tau_{m+1}]$, it holds that*

$$\begin{aligned} \frac{d^\alpha y}{dt^\alpha}(t_{n+1}) &= \sum_{k=0}^n d_{n+1,k} \frac{y(t_{k+1}^-) - y(t_k^+)}{t_{k+1} - t_k} \\ &\quad - \frac{1}{\Gamma(1-\alpha)} \sum_{j=1}^{m-1} \frac{y(\tau_j^+) - y(\tau_j^-)}{(t_{n+1} - \tau_j)^\alpha} + R_{n+1}, \end{aligned} \quad (17)$$

where

$$|R_{n+1}| \leq \frac{1}{\Gamma(1-\alpha)} (c_1 \Delta t_n^{1-\alpha} + c_2 \Delta t_{\max} \Delta t_n^{-\alpha}). \quad (18)$$

Proof. The derivation of the truncation error for the case where the spike times are not known follows ideas similar to the proof of [42, Theorem 4.2]. We show here the proof and highlight the differences. From Section 3, we have that

$$\frac{d^\alpha y}{dt^\alpha}(t_{n+1}) = \frac{1}{\Gamma(1-\alpha)} \left[\sum_{j=0}^{m-1} \int_{\tau_j}^{\tau_{j+1}} \frac{y'(s)}{(t_{n+1}-s)^\alpha} ds + \int_{\tau_m}^{t_{n+1}} \frac{y'(s)}{(t_{n+1}-s)^\alpha} ds \right],$$

for $t_{n+1} \in (\tau_m, \tau_{m+1}]$. For the current time step, we must separately consider the case where $\tau_m \in [t_n, t_{n+1}]$ and $\tau_m \notin [t_n, t_{n+1}]$. For simplicity, we only expand on the first case, where there is a discontinuity in the current interval. Then, we have that

$$\begin{aligned} & \sum_{j=0}^{m-1} \int_{\tau_j}^{\tau_{j+1}} \frac{y'(s)}{(t_{n+1}-s)^\alpha} ds + \int_{\tau_m}^{t_{n+1}} \frac{y'(s)}{(t_{n+1}-s)^\alpha} ds \\ &= \sum_{j=0}^{m-2} \int_{\tau_j}^{\tau_{j+1}} \frac{y'(s)}{(t_{n+1}-s)^\alpha} ds + \int_{\tau_{m-1}}^{t_n} \frac{y'(s)}{(t_{n+1}-s)^\alpha} ds \\ &+ \int_{t_n}^{\tau_m} \frac{y'(s)}{(t_{n+1}-s)^\alpha} ds + \int_{\tau_m}^{t_{n+1}} \frac{y'(s)}{(t_{n+1}-s)^\alpha} ds. \end{aligned}$$

On $[t_n, t_{n+1}]$ we can use a simple Taylor expansion to obtain a bound for the derivative. Due to the discontinuity, the expansion can only be $\mathcal{O}(1)$, which gives

$$\begin{aligned} & \int_{t_n}^{\tau_m} \frac{y'(s)}{(t_{n+1}-s)^\alpha} ds + \int_{\tau_m}^{t_{n+1}} \frac{y'(s)}{(t_{n+1}-s)^\alpha} ds \\ &= \tilde{d}_{n+1,n} \frac{y(t_{n+1}^-) - y(t_n^+)}{t_{n+1} - t_n} + \int_{t_n}^{t_{n+1}} \frac{R_{n,n+1}(s)}{(t_{n+1}-s)^\alpha} ds, \end{aligned}$$

where $\tilde{d}_{n+1,n} = \Gamma(1-\alpha)d_{n+1,n}$ and $|R'_{n,n+1}| < c$. If $\tau_m < t_n$, then the estimate $|R_{n,n+1}| < c\Delta t_n$ from [42] should be used. For the remaining intervals, we use the standard linear Lagrange interpolator of the L1 method. If the interval $[t_k, t_{k+1}]$ contains a discontinuity, the interpolation error is given by

$$y(s) = \frac{t_{k+1}-s}{t_{k+1}-t_k} y(t_k) + \frac{s-t_k}{t_{k+1}-t_k} y(t_{k+1}) + R_{k,k+1}(\xi),$$

for $\xi \in [t_k, t_{k+1}]$, where $|R_{k,k+1}| < c\Delta t_k$. A proof of this bound is found, for example, in [43, Lemma 5]. If the solution is continuous in the interval, then the bound from [42] applies again. Introducing this estimate into the integral, we have that

$$\begin{aligned} \alpha \int_{t_k}^{t_{k+1}} \frac{y(s)}{(t_{n+1}-s)^{1+\alpha}} ds &= \frac{y(s)}{(t_{n+1}-s)^\alpha} \Big|_{t_k}^{t_{k+1}} - \tilde{d}_{n+1,k} \frac{y(t_{k+1}^-) - y(t_k^+)}{t_{k+1} - t_k} \\ &+ \int_{t_k}^{t_{k+1}} \frac{R_{k,k+1}}{(t_{n+1}-s)^{1+\alpha}} ds. \end{aligned}$$

This expression can be used to give an error estimate for the remaining terms. We have, by integration by parts,

that

$$\begin{aligned}
& \sum_{j=0}^{m-2} \int_{\tau_j}^{\tau_{j+1}} \frac{y'(s)}{(t_{n+1}-s)^\alpha} ds + \int_{\tau_{m-1}}^{t_n} \frac{y'(s)}{(t_{n+1}-s)^\alpha} ds \\
&= \sum_{j=0}^{m-2} \left[\frac{y(s)}{(t_{n+1}-s)^\alpha} \Big|_{\tau_j}^{\tau_{j+1}} - \alpha \int_{\tau_j}^{\tau_{j+1}} \frac{y(s)}{(t_{n+1}-s)^{1+\alpha}} ds \right] \\
&+ \frac{y(s)}{(t_{n+1}-s)^\alpha} \Big|_{\tau_{m-1}}^{t_n} - \alpha \int_{\tau_{m-1}}^{t_n} \frac{y(s)}{(t_{n+1}-s)^{1+\alpha}} ds \\
&= \frac{y(s)}{(t_{n+1}-s)^\alpha} \Big|_{\tau_0}^{t_n} - \sum_{j=1}^{m-1} \frac{y(\tau_j^+) - y(\tau_j^-)}{(t_{n+1}-\tau_j)^\alpha} - \alpha \int_{\tau_0}^{t_n} \frac{y(s)}{(t_{n+1}-s)^{1+\alpha}} ds \\
&= \sum_{k=0}^{n-1} \tilde{d}_{n+1,k} \frac{y(t_{k+1}^-) - y(t_k^+)}{t_{k+1} - t_k} - \sum_{j=1}^{m-1} \frac{y(\tau_j^+) - y(\tau_j^-)}{(t_{n+1}-\tau_j)^\alpha} - \sum_{k=0}^{n-1} \int_{t_k}^{t_{k+1}} \frac{R_{k,k+1}(s)}{(t_{n+1}-s)^{1+\alpha}} ds.
\end{aligned}$$

The remainder can be determined by putting the results on $[0, t_n]$ and $[t_n, t_{n+1}]$ together to give

$$\begin{aligned}
|R_{n+1}| &= \frac{1}{\Gamma(1-\alpha)} \left| \int_{t_n}^{t_{n+1}} \frac{R_{n,n+1}(s)}{(t_{n+1}-s)^\alpha} ds - \sum_{k=0}^{n-1} \int_{t_k}^{t_{k+1}} \frac{R_{k,k+1}(s)}{(t_{n+1}-s)^{1+\alpha}} ds \right| \\
&\leq \frac{1}{\Gamma(1-\alpha)} (c_1 \Delta t_n^{1-\alpha} + c_2 \Delta t_{\max} \Delta t_n^{-\alpha}).
\end{aligned}$$

□

As we have seen in Theorem 6.1, the truncation error for the method is $O(1)$ and, thus, non-convergent. This is not surprising, due to the fact that the grid $\{t_n\}$ does not match the spike times $\{\tau_m\}$. However, the numerical convergence of the method is expected to be first order. We define the error as $e_n^\pm = y(t_n^\pm) - y_n^\pm$ and provide an estimate below.

Theorem 6.2 (Piecewise L1 Global Error). *Let the right-hand side $f(t, y)$ from (13) be Lipschitz continuous in its second argument, i.e.*

$$|f(t, x) - f(t, y)| < L|x - y|,$$

where $L > 0$ is the Lipschitz constant. Let $\{y_n^\pm\}$ be the numerical solution of (14) on a grid $0 = t_0 < \dots < t_n < \dots < t_N = T$ such that $\Gamma(2-\alpha)L\Delta t_n^\alpha < 1$ for every n . Then, the error satisfies

$$|e_{n+1}^-| < c\Delta t_{\max}.$$

Proof. To obtain an expression for the error, we subtract the residual equation from Theorem 6.1 from the discretization (7). This gives

$$\begin{aligned}
& e_{n+1}^- - h_{n+1} [f(t_{n+1}, y(t_{n+1}^-)) - f(t_{n+1}, y_{n+1}^-)] \\
&= e_n^+ - h_{n+1} \sum_{k=0}^{n-1} d_{n+1,k} \frac{e_{k+1}^- - e_k^+}{\Delta t_k} + \frac{h_{n+1}}{\Gamma(1-\alpha)} \sum_{j=1}^{m-1} \frac{y(\tau_j^+) - y(\tau_j^-)}{(t_{n+1}-\tau_j)^\alpha} - h_{n+1} R_{n+1}, \\
&= \left[1 - \frac{h_{n+1} d_{n+1,n-1}}{\Delta t_{n-1}} \right] e_n^- - h_{n+1} \sum_{k=1}^{n-1} \left[\frac{d_{n+1,k-1}}{\Delta t_{k-1}} e_k^- - \frac{d_{n+1,k}}{\Delta t_k} e_k^+ \right] \\
&+ \frac{h_{n+1}}{\Gamma(1-\alpha)} \sum_{j=1}^{m-1} \frac{y(\tau_j^+) - y(\tau_j^-)}{(t_{n+1}-\tau_j)^\alpha} - h_{n+1} R_{n+1}
\end{aligned}$$

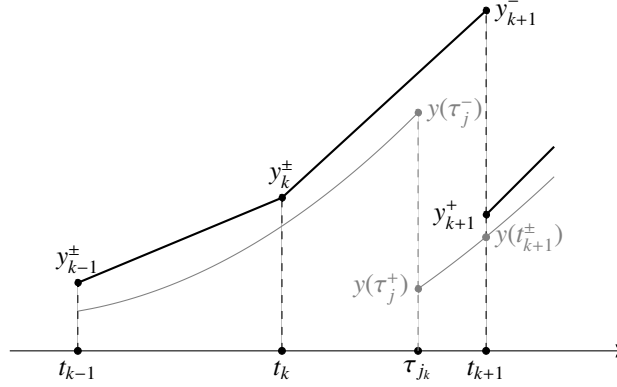


Figure 2: Approximate solution based on a linear approximation (black) and the exact solution (gray). The approximate solution has a detected jump at t_{k+1} and the exact solution has the jump at $\tau_j \in [t_{k-1}, t_{k+1}]$.

We must now manipulate the errors such that the jump terms cancel out to first order. In general, given a numerical spike time at t_k , we assume that the real spike time $\tau_{jk} \in [t_{k-1}, t_{k+1}]$, as shown in Figure 2. This can always be achieved if the step size is sufficiently small. Then, for each numerical spike time t_k , we can write

$$e_k^+ = (y(t_k^+) - y_k^+) = e_k^- - (y(\tau_{jk}^+) - y(\tau_{jk}^-)),$$

and introduce this expression into the error estimate

$$\begin{aligned} & h_{n+1} \sum_{k=1}^{n-1} \left[\frac{d_{n+1,k-1}}{\Delta t_{k-1}} e_k^- - \frac{d_{n+1,k}}{\Delta t_k} e_k^+ \right] - \frac{h_{n+1}}{\Gamma(1-\alpha)} \sum_{j=1}^{m-1} \frac{y(\tau_j^+) - y(\tau_j^-)}{(t_{n+1} - \tau_j)^\alpha} \\ &= h_{n+1} \sum_{k=1}^{n-1} \left[\frac{d_{n+1,k-1}}{\Delta t_{k-1}} - \frac{d_{n+1,k}}{\Delta t_k} \right] e_k^- \\ &+ h_{n+1} \sum_{j=1}^{m-1} \frac{d_{n+1,k_j}}{\Delta t_{k_j}} (y(\tau_j^+) - y(\tau_j^-)) - \frac{h_{n+1}}{\Gamma(1-\alpha)} \sum_{j=1}^{m-1} \frac{y(\tau_j^+) - y(\tau_j^-)}{(t_{n+1} - \tau_j)^\alpha}, \end{aligned}$$

where k_j denotes the numerical spike time t_{k_j} corresponding to τ_j , as denoted above. Now, we consider the weights in the second sum, as defined by (8), and perform the expansions

$$\begin{aligned} (t_{n+1} - t_k)^{1-\alpha} &= (t_{n+1} - \tau_j)^{1-\alpha} + (1-\alpha)(\tau_j - t_k)(t_{n+1} - \tau_j)^{-\alpha} + \mathcal{O}(\Delta t_k^2), \\ (t_{n+1} - t_{k+1})^{1-\alpha} &= (t_{n+1} - \tau_j)^{1-\alpha} - (1-\alpha)(t_{k+1} - \tau_j)(t_{n+1} - \tau_j)^{-\alpha} + \mathcal{O}(\Delta t_k^2), \end{aligned}$$

which give

$$\frac{d_{n+1,k}}{\Delta t_k} = \frac{1}{\Gamma(1-\alpha)} \frac{1}{(t_{n+1} - \tau_j)^\alpha} + \mathcal{O}(\Delta t_k).$$

We can see that the first term will exactly cancel out the original jump terms. Finally, using Theorem 6.1, we have that

$$\left| \frac{h_{n+1}}{\Gamma(1-\alpha)} R_{n+1} \right| \leq c_1 \Delta t_n + c_2 \Delta t_{\max}.$$

Therefore, we can write the error as

$$\begin{aligned}
& e_{n+1}^- - h_{n+1}[f(t_{n+1}, y(t_{n+1}^-)) - f(t_{n+1}, y_{n+1}^-)] \\
&= \left[1 - \frac{h_{n+1}d_{n+1,n-1}}{\Delta t_{n-1}} \right] e_n^- - h_{n+1} \sum_{k=1}^{n-1} \left[\frac{d_{n+1,k-1}}{\Delta t_{k-1}} - \frac{d_{n+1,k}}{\Delta t_k} \right] e_k^- \\
&- c_0 \sum_{j=0}^{m-1} \Delta t_k (y(\tau_j^+) - y(\tau_j^-)) + c_1 \Delta t_n + c_2 \Delta t_{\max} \\
&= \left[1 - \frac{h_{n+1}d_{n+1,n-1}}{\Delta t_{n-1}} \right] e_n^- - h_{n+1} \sum_{k=1}^{n-1} \left[\frac{d_{n+1,k-1}}{\Delta t_{k-1}} - \frac{d_{n+1,k}}{\Delta t_k} \right] e_k^- + c \Delta t_{\max},
\end{aligned}$$

for some positive constants $c_0, c_1, c_2, c \in \mathbb{R}$. We note that the last estimate can be invalid if the number of spike times becomes very large, i.e. if $m \max(y(\tau_j^+) - y(\tau_j^-)) = \mathcal{O}(\Delta t_{\max}^{-1})$. This can be the case if the solution is evolved for a very large time horizon.

We will now apply a variant of the discrete Grönwall inequality from [32, Lemma 3.3.1]. For this we first require some bounds on the coefficients of e_n^- . We have that

$$\begin{aligned}
\left| 1 - \frac{h_{n+1}d_{n+1,n-1}}{\Delta t_{n-1}} \right| &\leq 1 + \frac{\Delta t_n^\alpha}{\Delta t_{n-1}^\alpha} \leq 1 + C_{\Delta t}^\alpha, \\
h_{n+1} \left| \frac{d_{n+1,k-1}}{\Delta t_{k-1}} - \frac{d_{n+1,k}}{\Delta t_k} \right| &\leq \left| \frac{\Delta t_n^\alpha}{\Delta t_{k-1}^\alpha} - \frac{\Delta t_n^\alpha}{\Delta t_k^\alpha} \right| \leq 2C_{\Delta t}^\alpha.
\end{aligned}$$

Then, taking the absolute value on both sides and using the above bounds, we obtain

$$(1 - Lh_{n+1})|e_{n+1}^-| \leq c\Delta t_{\max} + \beta \sum_{k=0}^n |e_k^-|,$$

where $\beta \triangleq \max(1 + C_{\Delta t}^\alpha, 2C_{\Delta t}^\alpha)$. A direct application of the Grönwall inequality gives the desired result when $1 - Lh_{n+1} > 0$, as initially assumed. \square

Remark 6.1. *As shown in the proof of Theorem 6.2, we make very few assumptions on the form of the reset condition and the method of determining the numerical spike times $\{t_k\}$. Therefore, the error estimate applies not only to the FrAdEx discretization from Section 5, but also to a larger class of problems. For example, in the next section, we apply the same methods to the simpler perfect integrate-and-fire and the leaky integrate-and-fire models, where the spike times are approximated by a direct linear interpolation between (t_n, V_n^+) and $(\hat{t}_{n+1}, \hat{V}_{n+1}^-)$.*

Remark 6.2. *It is well-known that solutions to fractional differential equations (usually) have a singularity at $t = 0$ and we cannot generally assume that $y(t) \in \text{PAC}^2([0, T])$. More realistic spaces have been analysed for the L1 method [44] and for the L2 method [45]. In the case of the L1 method, the global error degrades to $\mathcal{O}(\Delta t)$ due to the singularity, as in Theorem 6.2.*

7. Numerical Simulations

We present a series of numerical experiments intended to verify and validate the numerical method presented in Section 5. The implementation is carried out in Python with the aid of the numpy and scipy version libraries.

The numerical method itself is implemented on top of `pycaputo` [46], an open source library for fractional calculus developed by the authors.

In the following, we will make use of the full machinery required to solve the FrAdEx model using adaptive time stepping and the implicit L1 method. All reported errors will be relative in the ℓ^2 norm, i.e.

$$E(\mathbf{x}, \mathbf{x}_{\text{ref}}) \triangleq \frac{\|\mathbf{x} - \mathbf{x}_{\text{ref}}\|_2}{\|\mathbf{x}_{\text{ref}}\|_2},$$

where \mathbf{x} is the approximate solution and \mathbf{x}_{ref} is a known reference value evaluated on the $\{t_n\}$ grid. The remaining parameters are problem-dependent and will be stated for each test case. In the text, they are stated in their dimensional form for comparison to existing literature [2], but the simulations are performed on the non-dimensional system from Section 4.

7.1. Convergence on a simple PIF model

We start by applying the methods from Section 5 to a simple perfect integrate-and-fire (PIF) model and use the results to verify the error estimates from Section 6. The fractional extension of the PIF model is given by

$$C \frac{d^\alpha V}{dt^\alpha} = I \quad \text{if } V < V_{\text{peak}} \quad \text{else } V \leftarrow V_r,$$

where $C = 100 \text{ pFms}^{\alpha-1}$ is the fractional capacitance, $I = 160 \text{ pA}$ is a constant current, $V_{\text{peak}} = 0 \text{ mV}$ is the membrane threshold potential, and $V_r = -48 \text{ mV}$ is the reset potential. The system is non-dimensionalized using $I_{\text{ref}} = 20 \text{ pA}$ and $V_{\text{ref}} = 1 \text{ mV}$. The initial condition is set to a random value in $[V_r, V_{\text{peak}}]$, fixed for each different order α tested below. This problem has a known solution, which is given by

$$V(t) = V_0 + m(V_r - V_{\text{peak}}) + \frac{t^\alpha}{\Gamma(1 + \alpha)} I,$$

for $t \in (\tau_m, \tau_{m+1}]$. The corresponding spike times also have an explicit expression

$$\tau_{m+1} = \sqrt[\alpha]{\Gamma(1 + \alpha) \frac{V_{\text{peak}} - V_0 - m(V_r - V_{\text{peak}})}{I}}.$$

This system also falls into the category described in Section 6 and the same error estimates apply. Therefore, we can test the accuracy of the given estimates for different orders α and different grid sizes. In the case of the PIF model, we can solve the implicit equation of the L1 method exactly and do not require the methods from Section 5.1. We also replace the adaptive spike time approximation with a simple linear interpolator: when $\hat{V}_{n+1}^- > V_{\text{peak}}$, we set

$$t_{n+1} = \frac{V_{\text{peak}} - V_n^+}{\hat{V}_{n+1}^- - V_n^+} \hat{t}_{n+1} + \frac{\hat{V}_{n+1}^- - V_{\text{peak}}}{\hat{V}_{n+1}^- - V_n^+} t_n$$

and proceed with the reset as described in Algorithm 1. To verify the method, we evolve the equation to a (non-dimensional) final time $T = 32$ using different $\alpha \in \{0.5, 0.75, 0.95\}$ and fixed time steps $\Delta t \in \{10^{-2}, 5 \times 10^{-3}, 10^{-3}, 5 \times 10^{-4}\}$. Note that the PIF model with a constant current I does not require adaptive time stepping, due to the function being very well-behaved away from $t = 0$. With these parameters, we have a total of 6 spike times. We can see in Figure 3 that we obtain the expected $O(\Delta t)$ order of convergence, due to the first-order estimate of the spike time locations.

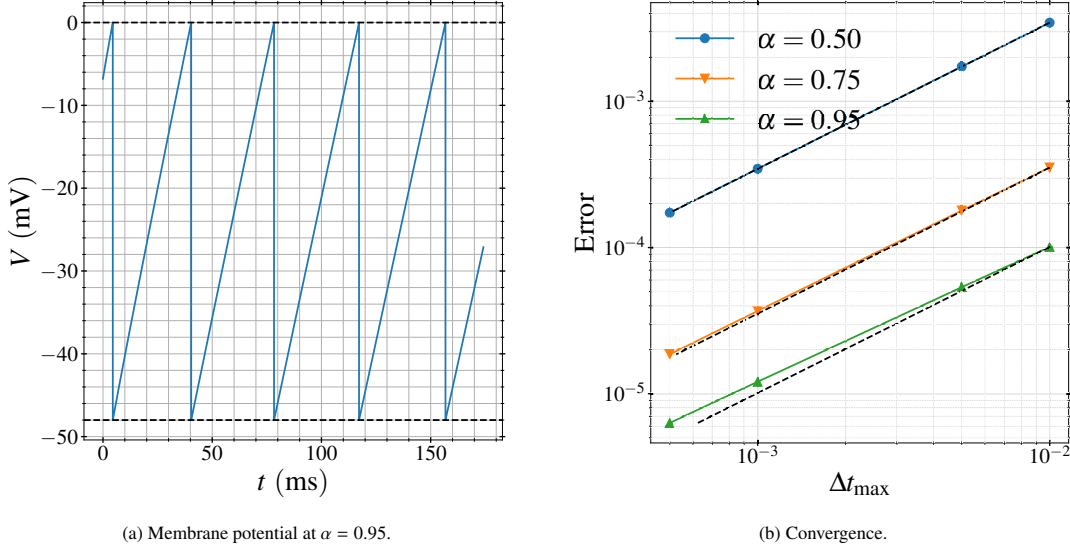


Figure 3: (a) Membrane potential at $\alpha = 0.95$ and $\Delta t = 5 \times 10^{-4}$. The peak potential V_{peak} and the reset potential V_r are denoted with dashed lines. (b) Convergence of the piecewise L1 method on the PIF model. The error is computed based on the location of the exact and the approximate spike times $\{\tau_m\}$. The dashed lines denote the expected order $O(\Delta t_{\text{max}})$.

7.2. Adaptivity of a simple LIF model

To briefly validate the step size adaptation presented in Section 5.3, we turn to the more complex leaky integrate-and-fire model (LIF). The fractional extension of the model is given by

$$C \frac{d^\alpha V}{dt^\alpha} = I - g_L(V - E_L) \quad \text{if } V < V_{\text{peak}} \quad \text{else } V \leftarrow V_r,$$

where $C = 100 \text{ pFms}^{\alpha-1}$ is the fractional capacitance, $I = 160 \text{ pA}$ is the constant current, $g_L = 3 \text{ nS}$ is the total leak conductance, $E_L = -50 \text{ mV}$ is the effective resting potential, $V_{\text{peak}} = 0 \text{ mV}$ is the peak membrane potential, and $V_r = -48 \text{ mV}$ is the reset potential. The system is non-dimensionalized using $V_{\text{ref}} = 1 \text{ mV}$ and $\alpha = 0.85$. As before, we evolve the equation to $T = 32$ (non-dimensional) with a linear approximation of the spike time, but using the adaptive time stepping method from Section 5.3.

For the adaptive algorithm, we set $\theta = 1.0$, $\sigma = 0.5$ and $\rho = 1.5$. The minimum time step is set to $\Delta t_{\text{min}} = 10^{-5}$ and the initial time step is taken to be $\Delta t_0 = 10^{-1}$. The remaining parameters χ_{min} and χ_{max} must be determined empirically to result in a stable and efficient adaptive scheme. In this experiment, we have chosen them in such a way that adaptivity is showcased for the simple LIF model. They are

$$\chi_{\text{min}} = \left\{ \frac{2}{2^k} \mid k = 0, 4, 8 \right\} \quad \text{and} \quad \chi_{\text{max}} = \left\{ \frac{4}{2^k} \mid k = 0, 4, 8 \right\}.$$

The results can be seen in Figure 4. At least on $[0, \tau_1]$, we know that the solution to the LIF model with constant current I is given by the Mittag-Leffler function, which in the limit of $\alpha \rightarrow 1$ becomes the exponential. Due to this smoothness of the solution, the time step is allowed to increase in a stepwise fashion until a new spike is near, when

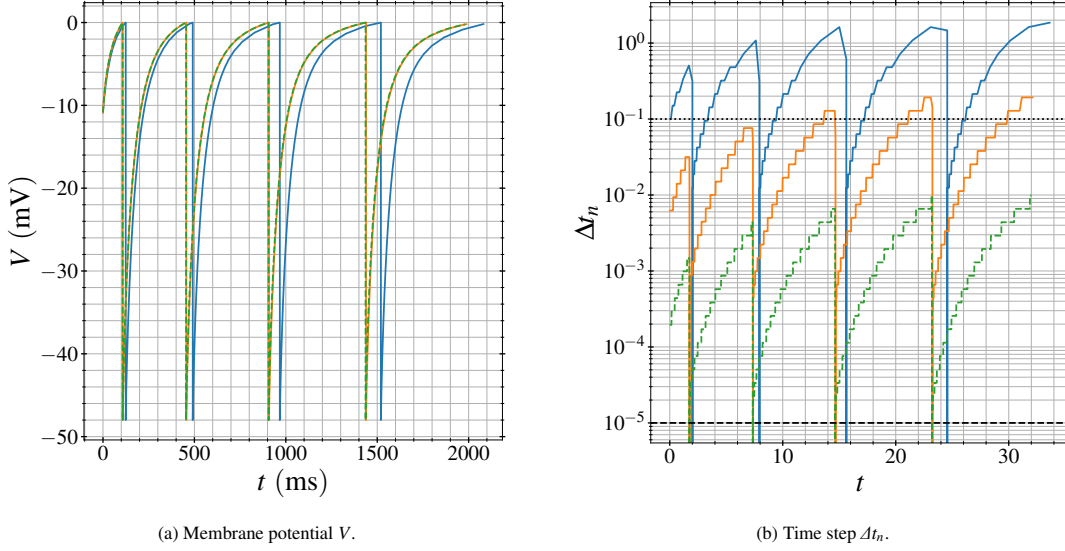


Figure 4: Evolution of the LIF model using an adaptive step size algorithm with $\Delta t_0 = 10^{-1}$ (dotted black) and $\Delta t_{\min} = 10^{-5}$ (dashed black). The bounds on the pointwise error are shown: $\chi_{\max} = 2^2$ (full), $\chi_{\max} = 2^{-2}$ (dashed) and $\chi_{\max} = 2^{-6}$ (dotted).

the linear interpolation results in a drastic decrease in the next step. As expected, the bounds $(\chi_{\min}, \chi_{\max})$ have a noticeable effect on the time step and allow for more accurate results. The convergence can be easily seen empirically in Figure 4a.

7.3. Convergence of the FrAdEx model

Having validated the behaviour of the numerical methods from Section 5 on simpler models, we can now continue to examine the convergence and performance of the more realistic FrAdEx model, for which we only consider the case $\alpha \equiv \alpha_1 = \alpha_2$. To verify the convergence of the model, we cannot compare to a known analytical solution, since no such solutions exist. However, we can compare to a significantly finer discretization of the equations, which is known as self-convergence.

As in Section 7.1, we will look at the convergence of the spike times and only perform the convergence study for one set of parameters with $\alpha = 0.9$. We take the fractional capacitance $C = 100 \text{ pFms}^{\alpha-1}$, the constant current $I = 160 \text{ pA}$, the total leak conductance $g_L = 3.0 \text{ nS}$, the effective resting potential $E_L = -50 \text{ mV}$, the effective threshold potential $V_T = -50 \text{ mV}$, the threshold slope factor $\Delta_T = 2 \text{ mV}$, the time constant $\tau_w = 150 \text{ ms}$, the conductance $a = 4 \text{ nS}$, the membrane threshold potential $V_{\text{peak}} = 0 \text{ mV}$, the reset potential $V_r = -48 \text{ mV}$, and the spike triggered adaptation $b = 120 \text{ pA}$. The systems is non-dimensionalized according to Section 4. The equation is evolved to $T = 50$ (non-dimensional) with an initial time step $\Delta t_0 = 10^{-2}$, and adaptive parameters $(\theta, \sigma, \rho) = (1, 0.5, 1.5)$. The adaptive error bounds are taken as

$$\chi_{\min} = \left\{ \frac{1}{2^k} \mid k \in \{0, \dots, 7\} \right\} \quad \text{and} \quad \chi_{\max} = \left\{ \frac{2}{2^k} \mid k \in \{0, \dots, 7\} \right\}.$$

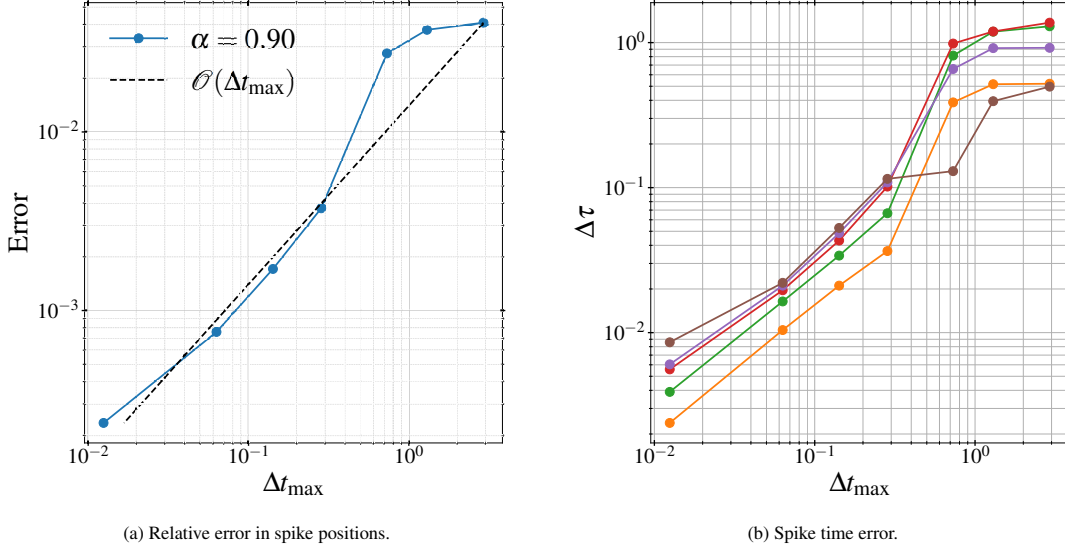


Figure 5: (a) First-order self-convergence of the FrAdEx model and (b) Pointwise error of each of the 5 numerical spike times for every $(\chi_{\min}, \chi_{\max})$ pair.

The convergence behaviour can be seen in Figure 5. As in the case of the simpler PIF model, we recover first-order convergence when comparing the finest solution with the coarser variants in our experiment. We can see in Figure 5b that the self-convergence error in each of the 5 spike times follows largely the same pattern and the errors for later spike times do not exhibit degraded convergence.

7.4. Performance on the FrAdEx model

Finally, we briefly investigate the efficiency of the L1 method that was implemented. We take the parameters from Section 7.3 and perform some standard performance and scaling studies for $\alpha = 0.9$. We expect $\alpha > 0.9$ in practical applications, since lower values of the fractional order do not present some irregular spiking behaviours, as shown in Section 8.

For the adaptive time-stepping, we take

$$\chi_{\min} = \left\{ \frac{1}{2^k} \mid k \in \{0, \dots, 7\} \right\} \quad \text{and} \quad \chi_{\max} = \left\{ \frac{2}{2^k} \mid k \in \{0, \dots, 7\} \right\},$$

with $\theta = 1.0, \sigma = 0.5, \rho = 2.0$ and a minimum time step of $\Delta t_{\min} = 10^{-5}$. The equation is evolved to $T = 50$ (non-dimensional) with an initial time step of $\Delta t_0 = 10^{-2}$. For comparison, we include simulations with a fixed step size and compare their accuracy. The fixed time step is taken as

$$\Delta t_{\text{fixed}} = \frac{T}{2N_{\text{adaptive}}},$$

where N_{adaptive} is the number of time steps taken by the adaptive algorithm. Note that even for the fixed step size evolution, we continue to restrict the time step close to a spike time to ensure that the Lambert W function remains

real, as discussed in Section 5.2. The error for both methods is computed by means of self-convergence as described in Section 7.3.

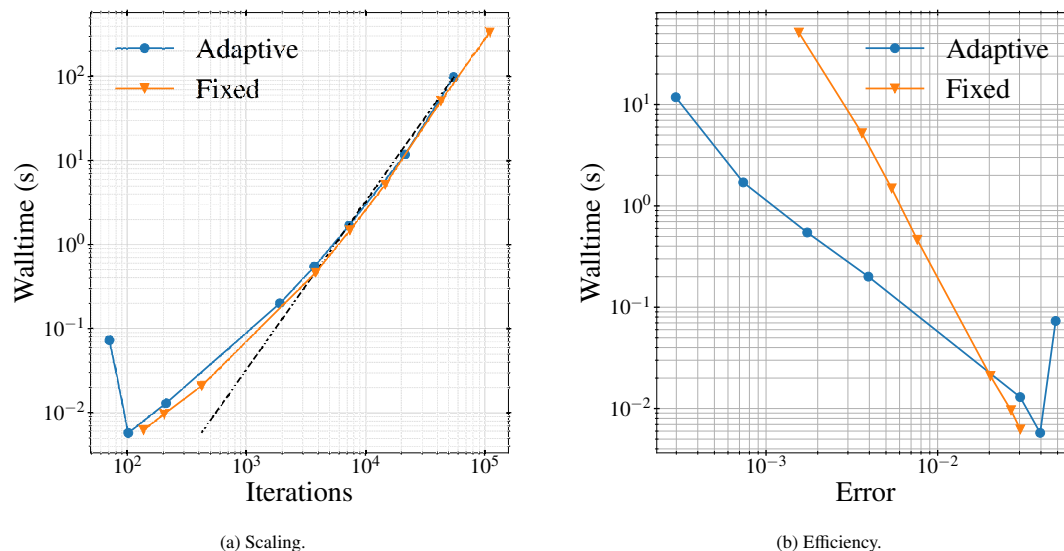


Figure 6: (a) Scaling of the L1 method with adaptive and fixed step sizes and (b) Efficiency of the method with adaptive and fixed step sizes, which is measured in the time required to reach a certain convergence error.

The results of the scaling study can be seen in Figure 6. First, in Figure 6a we can see that both methods scale with the expected $O(N^2)$ asymptotic order. This is due to the memory terms inherent in fractional-order equations. For smooth solutions, the scaling can be improved to $O(N \log N)$ with the use of Fourier transforms, but it is unclear if such methods could be used for non-uniform discontinuous systems. Then, in Figure 6b we can see that the fixed time step method generally performs significantly worse than the adaptive method. To obtain modestly small errors of 10^{-3} , it requires about an order of magnitude more time than the adaptive method. This is not surprising, since the fixed step method is unable to accurately capture the exponential spiking of the model.

8. Neural behaviour under the FrAdEx model

Finally, we look at simulating the fractional order FrAdEx model (5) with a focus on its phenomenological responses. We expect the model to generate multiple firing patterns depending on the choice of parameter values for different fractional exponents α . In order to study the range of firing responses accessible with the model, we adjust the fractional order α .

In Figure 7a, we show an example of a typical firing pattern known as *chattering* that is generated by setting the fractional order close to 1, e.g. $\alpha = 0.999$. The neuron exhibits stereotypical bursting of closely spaced spikes. As we decrease the fractional order to $\alpha = 0.98$, the pattern switches to a fast spiking with a broad spike after-potential (SAP) that is characterised by a small curvature after the spike (see Figure 7b). The fractional order FrAdEx model

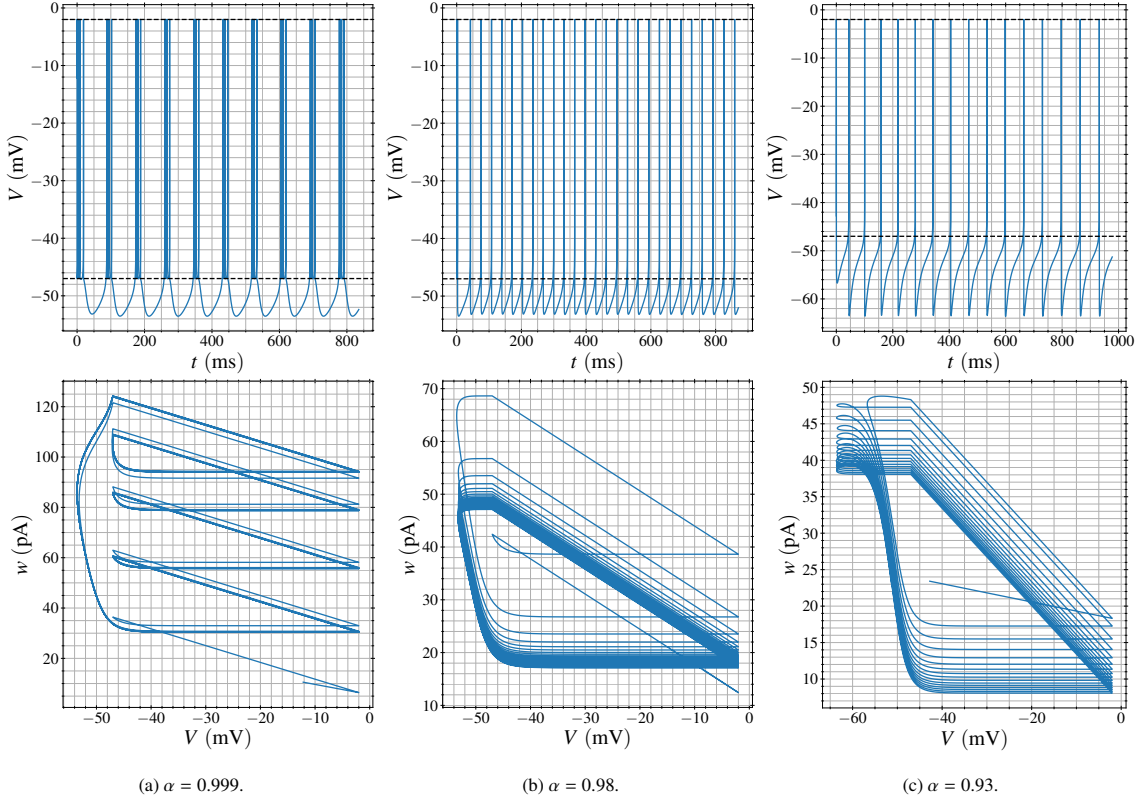


Figure 7: We have the evolution on $[0, 100]$ (non-dimensional) for different values of α of the membrane potential (top) and the phase plane diagram (bottom). The values of the parameters have been considered as follows $C = 100 \text{ pFms}^{\alpha-1}$, $I = 160 \text{ pA}$, $g_L = 12 \text{ nS}$, $E_L = -60 \text{ mV}$, $V_T = -50 \text{ mV}$, $\Delta_T = 2 \text{ mV}$, $\tau_w = 130 \text{ ms}$, $a = -11 \text{ nS}$, $b = 30 \text{ pA}$, $V_r = -48 \text{ mV}$, $V_{\text{peak}} = -2 \text{ mV}$ in the model (1).

can generate adapting and tonic traces of different types [47, 2]. As we decrease $\alpha = 0.93$, we can observe fast spiking without adaptation and with tonic spiking with sharp SAP. Here, the membrane potential increases monotonically after the rapid downswing of an action potential, as shown in Figure 7c. The corresponding phase diagrams also highlight these changes in behaviour, as seen at the bottom of Figure 7.

In Figure 8a, we use the same fractional order $\alpha = 0.999$ with another suitable set of parameters. We observe a regular discharge of action potential, i.e. tonic firing, and a broad spike after potential at this fractional order. However, the behaviour switches to regular spiking with sharp SAP at $\alpha = 0.98$ (see Figure 8b) and then spike frequency adaptation starts (i.e. the neurons fire a few spikes with short interspike interval and then the inter-spike period increases) at $\alpha = 0.93$ (see Figure 8c). The corresponding phase diagrams also highlight these changes in behaviour, as seen at the bottom of Figure 8.

For a final example, we look at another set of parameters Figure 9. Here, the fractional order FrAdEx model with $\alpha = 0.999$ can generate intrinsic bursting, initial bursting, and then single regular spikes are emitted (see Figure 9a). As we decrease α , we showed the transitions to tonic spiking with sharp SAP (see Figure 9b) and, finally, the model produces regular spiking with spike frequency adaptation at $\alpha = 0.93$ (see Figure 9c). The corresponding phase

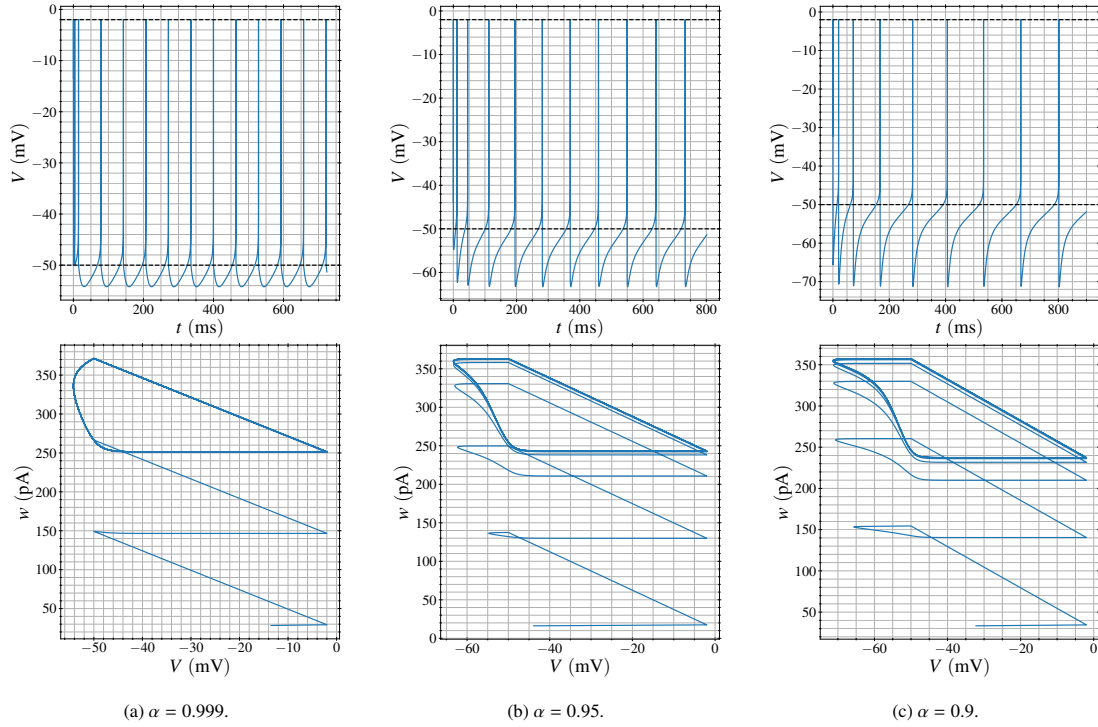


Figure 8: We have the evolution on $[0, 100]$ (non-dimensional) for different values of α of the membrane potential (top) and the phase plane diagram (bottom). The values of the parameters are taken to be $C = 130 \text{ pFms}^{\alpha-1}$, $I = 400 \text{ pA}$, $g_L = 18 \text{ nS}$, $E_L = -58 \text{ mV}$, $V_T = -50 \text{ mV}$, $\Delta_T = 2 \text{ mV}$, $\tau_w = 150 \text{ ms}$, $a = 4 \text{ nS}$, $b = 120 \text{ pA}$, $V_r = -50 \text{ mV}$, $V_{\text{peak}} = -2 \text{ mV}$ in the model (1).

diagrams also highlight these changes in behaviour, as seen at the bottom of Figure 9.

9. Conclusions

We have discussed the introduction of a novel fractional-order adaptive exponential (FrAdEx) integrate-and-fire model for neuronal activity. This model is a natural extension of popular adaptive exponential models that have proven to be representative of biophysical neurons. We have shown that the fractional extension can also reproduce some sought after phenomenology, such as chattering or tonic spiking of the neuron. Furthermore, we have shown that the fractional order α can be used to control the behaviour of the neuronal spiking. We know that decreasing the fractional order is equivalent to putting more weight on the memory property of the fractional derivative. In our experiments, this has resulted in a more regular bursting pattern, which is consistent with similar simulations of the fractional LIF model. On the other hand, in the limit of $\alpha \rightarrow 1$, the model will recover the integer order behaviour. Due to its complexity and wide parameter ranges, we have not fully investigated the full response capabilities that the FrAdEx model can achieve. This requires a more careful theoretical analysis that is in preparation. However, we do expect that some types of irregular spiking can only be expected in the limit of sufficiently large α .

The main contribution of this paper is the numerical investigation of the FrAdEx model. For this, we have intro-

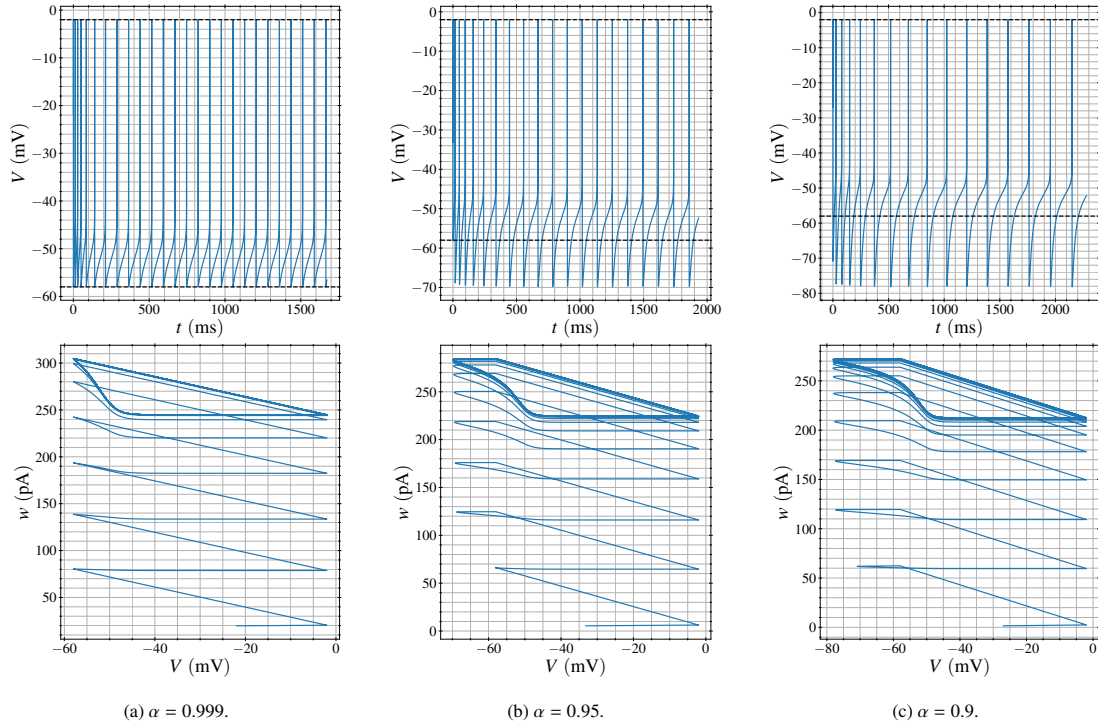


Figure 9: We have the evolution on $[0, 100]$ (non-dimensional) for different values of α of the membrane potential (top) and the phase plane diagram (bottom). The values of the parameters are taken to be $C = 200 \text{ pFms}^{\alpha-1}$, $I = 500 \text{ pA}$, $g_L = 12 \text{ nS}$, $E_L = -70 \text{ mV}$, $V_T = -50 \text{ mV}$, $\Delta_T = 2 \text{ mV}$, $\tau_w = 300 \text{ ms}$, $a = 2 \text{ nS}$, $b = 60 \text{ pA}$, $V_r = -58 \text{ mV}$, $V_{\text{peak}} = -2 \text{ mV}$ in the model (1).

duced a novel adaptive implicit L1-type numerical method that we have fully described. As expected, at the numerical level, the main difficulties have been the rapid exponential growth of the voltage V and the state-dependent rest conditions that the integrate-and-fire models are known for. The exponential growth has been dealt with by making use of an implicit method, which we have managed to solve efficiently through the use of the Lambert W function. Previous experiments with explicit methods have not yielded satisfactory results for this problem. The discontinuous reset condition is mainly handled through the use of the non-uniform L1 method and adaptive time stepping. This allows for a robust approach to the discontinuity during the exponential growth and an accurate estimate of the spike times themselves. We have also presented a complete error model of the method that can be directly applied to other integrate-and-fire models. This method has been validated on several benchmark examples that show the expected first-order convergence.

In the case of integer-order models, higher-order methods for discontinuous ODEs are well-known. We expect to extend the method described here to second-order for integrate-and-fire models with modest growth leading to the spike. For example, many PIF and LIF models could be treated by using a higher-order interpolation of the spike times and the solutions as a reset is detected. However, the exponential models are significantly more difficult to handle, as it is unclear how a more accurate approximation of the discontinuities can be achieved in the fractional derivative.

Another important avenue of research pertains to considering networks of neurons described by the FrAdEx model. Depending on the coupling of the neurons, explicit solutions based on the Lambert W function may not be possible and adaptive time stepping methods may require additional modifications to handle the small steps leading to a spike. Some of these issues are common to all fractional neuron models and will no doubt see ample research in the future.

Acknowledgements. This work was supported in part by West University of Timișoara, Romania, START Grant No. 33580/25.05.2023 (Fikl). This work was supported in part by CNCS-UEFISCDI, Romania, Project No. PN-IV-P1-PCE2023-0444 (Kaslik). This work was supported in part by CSIR-HRDG, Govt. of India under Grant No. 25/0322/23/EMR-II (Mondal).

Declaration of Interests. The authors report no conflict of interest.

References

- [1] R. Brette, W. Gerstner, Adaptive exponential integrate-and-fire model as an effective description of neuronal activity, *Journal of Neurophysiology* 94 (5) (2005) 3637–3642. doi:10.1152/jn.00686.2005.
- [2] R. Naud, N. Marcille, C. Clopath, W. Gerstner, Firing patterns in the adaptive exponential integrate-and-fire model, *Biological Cybernetics* 99 (2008) 335–347. doi:10.1007/s00422-008-0264-7.
- [3] J. Touboul, R. Brette, Dynamics and bifurcations of the adaptive exponential integrate-and-fire model, *Biological Cybernetics* 99 (4) (2008) 319–334. doi:10.1137/070687268.
- [4] E. M. Izhikevich, *Dynamical systems in neuroscience*, MIT Press, 2007.
- [5] L. Lapicque, Recherches quantitatives sur l’excitation électrique des nerfs, *Journal de physiologie et de pathologie générale* 9 (1907) 620–635.
- [6] T. Górski, D. Depannemaecker, A. Destexhe, Conductance-based adaptive exponential integrate-and-fire model, *Neural Computation* 33 (1) (2021) 41–66. doi:10.1162/neco_a_01342.
- [7] W. Teka, T. M. Marinov, F. Santamaria, Neuronal spike timing adaptation described with a fractional leaky integrate-and-fire model, *PLoS Computational Biology* 10 (3) (2014). doi:10.1371/journal.pcbi.1003526.
- [8] E. M. Izhikevich, Simple model of spiking neurons, *IEEE Transactions on Neural Networks* 14 (6) (2003) 1569–1572. doi:10.1109/tnn.2003.820440.
- [9] W. Gerstner, W. M. Kistler, R. Naud, L. Paninski, *Neuronal dynamics: From single neurons to networks and models of cognition*, Cambridge University Press, 2014.
- [10] P. Lansky, S. Ditlevsen, A review of the methods for signal estimation in stochastic diffusion leaky integrate-and-fire neuronal models, *Biological Cybernetics* 99 (4-5) (2008) 253–262. doi:10.1007/s00422-008-0237-x.
- [11] N. Fourcaud-Trocmé, D. Hansel, C. V. Vreeswijk, N. Brunel, How spike generation mechanisms determine the neuronal response to fluctuating inputs, *Journal of Neuroscience* 23 (37) (2003) 11628–11640. doi:10.1523/jneurosci.23-37-11628.2003.
- [12] E. M. Izhikevich, Which model to use for cortical spiking neurons?, *IEEE Transactions on Neural Networks* 15 (5) (2004) 1063–1070. doi:10.1109/tnn.2004.832719.
- [13] A. A. Prinz, C. P. Billimoria, E. Marder, Alternative to hand-tuning conductance-based models: construction and analysis of databases of model neurons, *Journal of Neurophysiology* (2003). doi:10.1152/jn.00641.2003.
- [14] P. Dayan, L. F. Abbott, *Theoretical neuroscience: Computational and mathematical modeling of neural systems*, MIT Press, 2005.
- [15] C. Clopath, R. Jolivet, A. Rauch, H.-R. Lüscher, W. Gerstner, Predicting neuronal activity with simple models of the threshold type: Adaptive exponential integrate-and-fire model with two compartments, *Neurocomputing* 70 (10-12) (2007) 1668–1673. doi:10.1016/j.neucom.2006.10.047.

- [16] D. L. M. Souza, E. C. Gabrick, P. R. Protachevicz, F. S. Borges, J. Trobia, K. C. Iarosz, A. M. Batista, I. L. Caldas, E. K. Lenzi, Adaptive exponential integrate-and-fire model with fractal extension, *Chaos: An Interdisciplinary Journal of Nonlinear Science* 34 (2) (2024). doi:10.1063/5.0176455.
- [17] I. Podlubny, *Fractional differential equations: an introduction to fractional derivatives, fractional differential equations, to methods of their solution and some of their applications*, Elsevier, 1998.
- [18] S. G. Samko, A. A. Kilbas, O. I. Marichev, et al., *Fractional integrals and derivatives*, Vol. 1, Gordon and Breach, 1993.
- [19] C. Li, G. Peng, Chaos in Chen's system with a fractional order, *Chaos, Solitons & Fractals* 22 (2004) 443–450. doi:https://doi.org/10.1016/j.chaos.2004.02.013.
- [20] Y. Yu, H.-X. Li, S. Wang, J. Yu, Dynamic analysis of a fractional-order lorenz chaotic system, *Chaos, Solitons & Fractals* 42 (2009) 1181–1189. doi:https://doi.org/10.1016/j.chaos.2009.03.016.
- [21] R. Hilfer, *Threefold introduction to Fractional Derivatives*, Wiley-VCH, 2008, Ch. 2, pp. 17–74. doi:10.1002/9783527622979.
- [22] R. Metzler, J. Klafter, The random walk's guide to anomalous diffusion: a fractional dynamics approach, *Physics Reports* 339 (1) (2000) 1–77. doi:10.1016/s0370-1573(00)00070-3.
- [23] C. Ionescu, A. Lopes, D. Copot, J. A. T. Machado, J. H. T. Bates, The role of fractional calculus in modeling biological phenomena: A review, *Communications in Nonlinear Science and Numerical Simulation* 51 (2017) 141–159. doi:10.1016/j.cnsns.2017.04.001.
- [24] T. A. M. Langlands, B. I. Henry, S. L. Wearne, Fractional cable equation models for anomalous electrodiffusion in nerve cells: Finite domain solutions, *SIAM Journal on Applied Mathematics* 71 (2011) 1168–1203. doi:10.1137/090775920.
- [25] R. L. Magin, Fractional calculus models of complex dynamics in biological tissues, *Computers & Mathematics with Applications* 59 (5) (2010) 1586–1593. doi:10.1016/j.camwa.2009.08.039.
- [26] G. Gilboa, R. Chen, N. Brenner, History-dependent multiple-time-scale dynamics in a single-neuron model, *Journal of Neuroscience* 25 (28) (2005) 6479–6489. doi:10.1523/jneurosci.0763-05.2005.
- [27] S. H. Weinberg, F. Santamaria, History dependent neuronal activity modeled with fractional order dynamics, *Computational Models of Brain and Behavior* (2017) 531–548doi:10.1002/9781119159193.ch39.
- [28] Y. Deng, B. Liu, Z. Huang, X. Liu, S. He, et al., Fractional spiking neuron: Fractional leaky integrate-and-fire circuit described with dendritic fractal model, *IEEE Transactions on Biomedical Circuits and Systems* 16 (2022) 1375–1386. doi:10.1109/tbcas.2022.3218294.
- [29] J. Wang, M. Fečkan, Y. Zhou, A survey on impulsive fractional differential equations, *Fractional Calculus and Applied Analysis* 19 (4) (2016) 806–831. doi:10.1515/fca-2016-0044.
- [30] V. Lakshmikantham, S. Leela, S. Kaul, Comparison principle for impulsive differential equations with variable times and stability theory, *Nonlinear Analysis: Theory, Methods & Applications* 22 (1994) 499–503. doi:10.1016/0362-546x(94)90170-8.
- [31] S. Yang, C. Li, T. Huang, State-dependent impulsive synchronisation of complex dynamical networks with non-linear coupling, *IET Control Theory & Applications* 12 (9) (2018) 1189–1200. doi:10.1049/iet-cta.2017.0909.
- [32] C. Li, F. Zeng, *Numerical methods for fractional calculus*, Vol. 24, CRC Press, 2015.
- [33] A. Jannelli, A novel adaptive procedure for solving fractional differential equations, *Journal of Computational Science* 47 (2020) 101220–101220. doi:10.1016/j.jocs.2020.101220.
- [34] M. J. Shelley, L. Tao, Efficient and accurate time-stepping schemes for integrate-and-fire neuronal networks, *Journal of Computational Neuroscience* 11 (2001) 111–119. doi:10.1023/a:1012885314187.
- [35] Z. Li, Z. Liang, Y. Yan, High-order numerical methods for solving time fractional partial differential equations, *Journal of Scientific Computing* 71 (2017) 785–803. doi:10.1007/s10915-016-0319-1.
- [36] Z. Yang, F. Zeng, A corrected II method for a time-fractional subdiffusion equation, *Journal of Scientific Computing* 95 (2023). doi:10.1007/s10915-023-02204-7.
- [37] S. Westerlund, L. Ekstam, Capacitor theory, *IEEE Transactions on Dielectrics and Electrical Insulation* 1 (5) (1994) 826–839. doi:10.1109/94.326654.
- [38] A. A. Kilbas, H. M. Srivastava, J. J. Trujillo, *Theory and applications of fractional differential equations*, Vol. 204, Elsevier, 2006.

- [39] M. Fečkan, Y. Zhou, J. Wang, On the concept and existence of solution for impulsive fractional differential equations, *Communications in Nonlinear Science and Numerical Simulation* 17 (2012) 3050–3060. doi:10.1016/j.cnsns.2011.11.017.
- [40] Y. Liu, R. Agarwal, Existence of solutions of bvps for impulsive fractional langevin equations involving caputo fractional derivatives, *Turkish Journal of Mathematics* 43 (2019) 2451–2472. doi:10.3906/mat-1905-23.
- [41] E. Hairer, G. Wanner, *Solving Ordinary Differential Equations II - Stiff and Differential-Algebraic Problems*, Springer, 2010.
- [42] C. Li, M. Cai, *Theory and numerical approximations of fractional integrals and derivatives*, SIAM, 2019.
- [43] H. T. Nguyen, M. N. Do, Error analysis for image-based rendering with depth information, *IEEE Transactions on Image Processing* 18 (2009) 703–716. doi:10.1109/tip.2009.2012884.
- [44] B. Jin, R. Lazarov, Z. Zhou, An analysis of the l1 scheme for the subdiffusion equation with nonsmooth data, *IMA Journal of Numerical Analysis* (2015). doi:10.1093/imanum/dru063.
- [45] C. Quan, X. Wu, Global-in-time H^1 -stability of L^2 - 1_σ method on general nonuniform meshes for subdiffusion equation, *Journal of Scientific Computing* 95 (2023). doi:10.1007/s10915-023-02184-8.
- [46] A. Fikl, *pycaputo v0.5.0* (2024). doi:10.5281/zenodo.10996100.
- [47] B. W. Connors, M. J. Gutnick, Intrinsic firing patterns of diverse neocortical neurons, *Trends in Neurosciences* 13 (3) (1990) 99–104. doi:10.1016/0166-2236(90)90185-d.